J Appl Electrochem (2014) 44:701–707
DOI 10.1007/s10800-014-0680-4

RESEARCH ARTICLE

Controlling the thickness of electrochemically produced porous alumina membranes: the role of the current density during the anodization

A. Christoulaki · S. Dellis · N. Spiliopoulos · D. L. Anastassopoulos · A. A. Vradis

Received: 10 December 2013 / Accepted: 5 March 2014 / Published online: 19 March 2014

Abstract A study of the thickness growth rate of anodized porous alumina membranes (PAMs) and its connection to the current density during the anodization process is presented. Several samples of PAMs were prepared in a hydrate solution of 0.3 M oxalic acid, under applied voltages of 40 and 50 V with varying solution temperatures in a purpose-built electrochemical cell. The thickness of the PAMs produced under these conditions was measured using cross section images taken by scanning electron microscopy (SEM). From these measurements, a linear expression between the growth rate of PAMs and the current density during the anodization is deduced, giving an efficiency value of 53 and 65 % for applied voltages 40 and 50 V, respectively. In steady state conditions, i.e., after the stabilization of the anodization current, this linear dependence is very conveniently transformed into linear dependence of thickness versus total anodization time, providing thus a simple method for controlling the thickness of the produced membranes. Finally, from the Arrhenius-type plot of the thickness growth rate versus temperature and the anodization current density vs temperature a mean value of 48.5 kJ mol^{-1} for the aluminum oxide formation activation energy E_a is deduced.

Keywords Porous alumina · Anodization · Activation energy · Growth rate

A. Christoulaki · S. Dellis · N. Spiliopoulos · D. L. Anastassopoulos · A. A. Vradis (✉)
Department of Physics, University of Patras, Rion, GR26504 Patras, Greece
e-mail: vradis@physics.upatras.gr

1 Introduction

Porous anodic alumina membranes formed under aluminum anodic oxidation have received particular attention over the past 20 years due to their wide range of applications in optical, magnetic, and electric nano-devices, and their use as filters or templates for the fabrication of nanowires, nanotubes, and chemical sensors [1–8]. The membrane morphology is crucial for each particular application; hence, precise control during the fabrication process is of major importance. The morphology of PAMs is basically described by four parameters, the mean pore diameter (D_p), the inter-pore distance (D_{int}), the barrier layer thickness (L_b), and the thickness of the membrane (h). The dependence of the D_p, D_{int}, and L_b on the anodization parameters has been described in detail in a number of studies [9–14]. It is widely accepted that these three parameters are proportional to the applied voltage with the proportionality constant ranging from 1 to 1.5 nm V^{-1} for D_p [9, 10], from 2 to 2.5 nm V^{-1} for D_{int} [11, 12], and from 1 to 1.3 nm V^{-1} for L_b [13, 14].

Several attempts have appeared in the literature in order to explore the mechanism of pore formation during aluminum anodization [15–17]. Proposed mechanisms can be basically distinguished as based on (i) field assisted dissolution, (ii) oxygen bubble effect, and (iii) stress driven viscous oxide flow.

According to the model of field assisted dissolution, the oxide grows at the metal/oxide interface due to counter migration of Al^{3+}, O^{2-}, and field assisted dissolution of the alumina at the oxide/electrolyte interface. In contrast to chemical dissolution, field assisted dissolution involves the breakage of the Al–O bond with the aid of an external electric field. Increased current density at the bottom of the alumina pores raises the temperature locally easing thus the

dissolution [18]. The initial pore growth sites are ridges, grooves, and other surface irregularities that pre-exist on the aluminum surface at the beginning of the anodization [19].

In the oxygen bubble effect model, oxygen bonded in the alumina structure undergoes conversion to oxygen gas either at the oxide bulk or at the oxide/electrolyte interface [20]. Additionally, the Al^{3+} ions released during this process are ejected from the oxide/electrolyte interface where they react with electrolyte anions [21]. Oxygen gas evolution initially takes place at impurity center sites or at defect sites with local high lattice stress leading to small pores formation. Oxygen gas generated this way causes the formation of bubbles exerting an isotropic pressure at the metal oxide interface. The oxide layer erupts under this pressure, and the barrier layer is dissolved. Repeated cycles of this procedure lead to the eventual formation of the pores. It is not yet very clear though through which mechanism, the oxygen ion loses electrons in order to be transformed to oxygen gas. A possible explanation of the oxide conductivity required for the above electron transfer is the ionization via a Pool–Frenkel mechanism of the incorporated species in the aluminum oxide originated from the free radicals of the electrolyte [20].

A slight variation of this model [22] adopts the migration of aluminum as neutral atoms (Al) and not as aluminum cations (Al^{3+}). Al atoms, reach the interface where they react with protons, converting to Al^{3+}.

The stress viscous oxide flow model is recently introduced [23, 24]. According to this model, pores grow both due to ionic migration through the oxide and creep from the oxide toward the pore walls. The latter is a consequence of mechanical stress gradients arising inside the oxide bulk. More specifically, this compressive stress arises through the competition of incoming O^{2-} at the pore bottom with the electrolyte anions adsorbed at the surface. This mechanism has been confirmed both by simulations and experimentally, observing the movement of tracers. Another possible cause of this mechanical stress is the pressure exerted by the oxygen bubbles at the electrolyte/oxide interface, generated in a similar manner to that observed in solid oxide electrolyte cells [25].

Although thickness is a key parameter for a number of applications, the growth rate of PAM under potentiostatic anodization conditions is not studied as extensively as pore formation. In a recent work by Zaraska et al. [26], the effect of the anodization parameters on the PAM geometrical characteristics has been studied in detail. The anodization time versus the final thickness of PAMs fabricated under a variety of anodization conditions has been established in the above work. Although the extracted relation is very useful for estimating the thickness of the PAM, it is restricted to a number of specific anodization conditions and cannot be of more general use. Therefore, the need of establishing a relationship connecting the growth rate of PAM thickness with a more general anodization parameter remains very important to the ever-growing PAM community. It is widely known that different anodization parameters as for example the kind and temperature of the electrolyte have a direct effect on the current density transferred through the electrochemical cell. Obviously, the geometrical characteristics of the cell itself (such as the size and distance between the electrodes) have also an effect on current density. Current density is a parameter that can always be calculated independently of other experimental conditions. Therefore, the investigation of its relationship to the growth rate of PAMs could lead to a useful tool for the control of the final thickness of the membrane in a universal way, i.e., under any experimental conditions.

2 Experimental set up

For the experimental requirements of this work, an electrochemical cell has been designed (Fig. 1). PTFE has been chosen for the cell construction, a material combining substantial thermal and chemical resistance. The cell is filled with the electrolyte solution which comes into contact with the Al foil to be anodized via a 22-mm hole drilled in the bottom of the cell and sealed with an o-ring. A nickel grid (60 mesh) serves as the cathode electrode, while the Al foil is connected to the anode via a spring loaded contact. The cell with the sample fitted is placed on a Peltier cold plate with adjustable temperature settings.

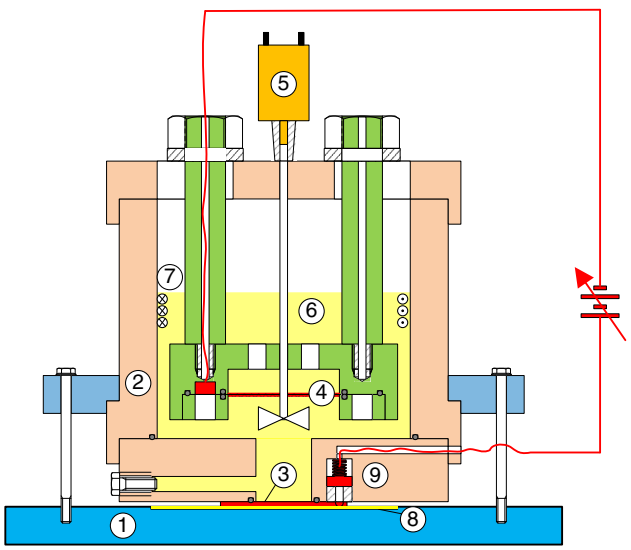

Fig. 1 Schematic representation of the experimental setup. *1* cold plate, *2* PTFE cell, *3* Al foil sample, *4* nickel electrode, *5* motor stirrer, *6* electrolyte solution, *7* heat exchanging coil, *8* thin electrical insulating membrane, and *9* spring loaded contact

Furthermore, the electrolyte solution is always kept at a constant temperature with the aid of a heat exchanging circuit immersed in the solution which is also continuously stirred by a motor stirrer attached on the cap of the cell. A thin plastic membrane is fitted between the sample and the cold plate for electrical insulation purposes.

3 Experimental procedure

High purity aluminum foil (99.99 %) was used for the fabrication of PAMs. Prior to anodization the aluminum foil's surface received an electropolishing treatment at 60 °C for 60 s under an applied voltage of 20 V. The electropolish solution consisted of H_3PO_4, H_2SO_4, and distilled water in 4:4:2 (v/v), and the procedure was followed by washing the aluminum with distilled water and ethanol. Then, the anodization of the Al foil takes place in a hydrate solution of 0.3 M oxalic acid for applied voltages 40 and 50 V. In order to determine the porosity and the density of PAMs with adequate accuracy, the two-step anodization method was used as the pores formed during the second step of anodization is regularly distributed. Furthermore, there is no difference in oxide growth rate for the first and second anodizing step [27]. After the post-anodization chemical dissolution of the oxide, the alumina density was calculated by a gravitational method which resulted to a value of 3.1 g cm^{-3}. The porosity was estimated to 20 % for 40 V and 16 % for 50 V from SEM images with an error of 2 % for all samples. The duration of the anodization procedure varied between 3 and 4 h, while the temperature was kept constant for each PAM and varied from −0.5 °C upto 20 °C, which falls in the region of mild anodization conditions. Special precaution must be taken in order to accurately stabilize the temperature during the anodization procedure since the exothermic nature of the reactions taking place inside an electrochemical cell tends to increase the temperature resulting to the increase of the current density. Fresh electrolyte solution was always used, in order to avoid extra Al^{3+} remaining from previous anodizations that could contribute to the measured current and lead to erroneous values for the current density. The thickness of the produced membranes was measured using cross sectional views of scanning electron microscopy (SEM). In Fig. 2a, it is clear that porous alumina growth is uniform throughout the sample's section. The porosity was measured from top views of samples formed by a two-step anodization process (Fig. 2b, c).

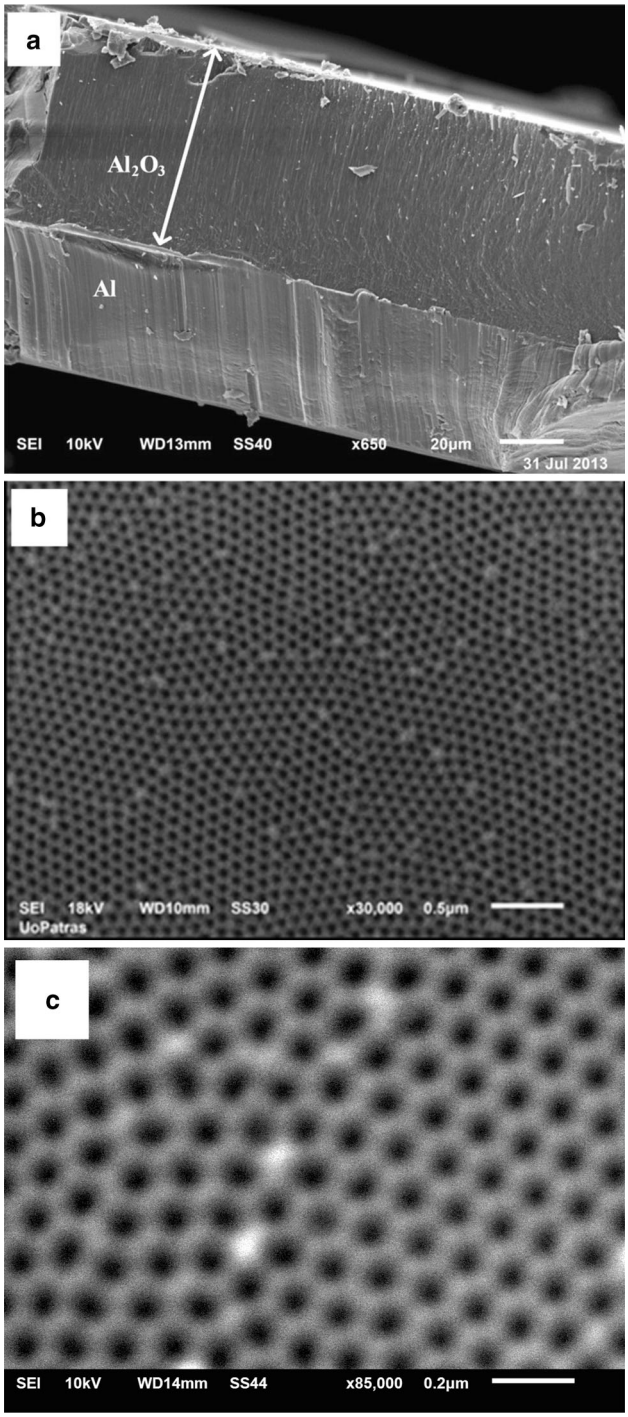

Fig. 2 SEM images **a** section view of PAM fabricated under 40 V, 7.5 °C with its aluminum substrate. **b** Top view of a sample after 2-step anodization under 40 V, 5 °C, 4 h. **c** Top view of a sample after 2-step anodization under 50 V, 14 °C, 3 h

4 Results–discussion

In Fig. 3, a typical current density graph against anodization time is presented. Within several seconds from the onset of the anodization, the current reaches a constant value, indicating that the aluminum oxide growth rate is stable over time.

The measured current corresponds primarily to the movement of O^{2-} anions arriving at the metal/oxide

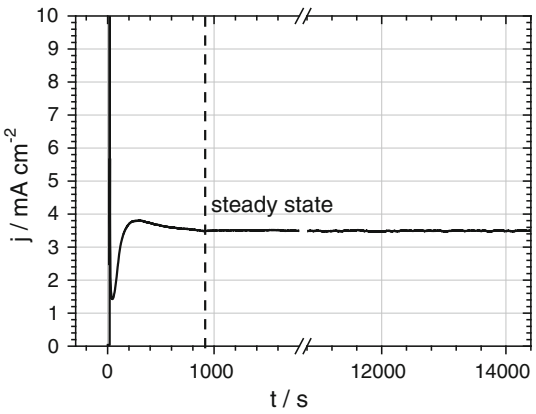

Fig. 3 Current versus time graph for anodized sample at 40 V and 7.5 °C

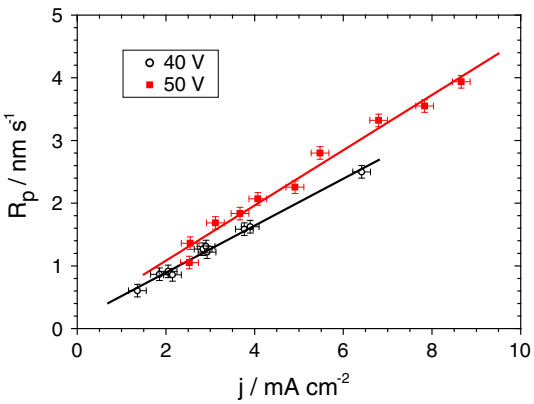

Fig. 4 Plot of thickness growth rate R_p versus steady state current density j for the samples anodized under 40 and 50 V in 0.3 M oxalic acid and at temperatures varying from −0.5 °C upto 20 °C

interface and also to the current of Al^{3+} cations which are ejected to the electrolyte. At the metal/oxide interface, Al^{3+} cations are formed and their mass $m_{Al^{3+}}$ according to Faraday's law is

$$m_{\left(Al^{3+}\right)_{n=100\%}} = \frac{M_{Al}}{z\,F}\; i\; t \tag{1}$$

where M_{Al} is the molar mass of aluminum, i is the total current of the anodization, t is the duration of the process, F is Faraday's constant, and z the number of electrons involved in the reaction. Three electrons are produced in the aluminum oxidation process ($z = 3$), while at the anode, two O^{2-} convert to O_2 gas by losing four electrons. Some of the Al^{3+} ions migrate through the bulk of the oxide and reach the oxide/electrolyte interface and are ejected directly into the solution, not participating in the formation of the oxide. Reaction of oxygen evolution and possible migration of aluminum cations contributes to the current measured at the external circuit not taking part into the oxide formation. Thus, the obtained mass of porous oxide according to Faraday's law is

$$m_p = \frac{M_{Al_2O_3}}{z\,F}\; i_{o^{2-}}\; t = \frac{M_{Al_2O_3}}{z\,F}\; i\; T_{o^{2-}}\; t \tag{2}$$

where $M_{Al_2O_3}$ is the molar mass of Al_2O_3, z = 6 in this case, and $T_{O^{2-}}$ the transport number of O^{2-},

$$T_{o^{2-}} = \frac{i_{o^{2-}}}{i} \tag{3}$$

The transport number $T_{O^{2-}}$ is the fraction of current carried by the O^{2-} anions, and it is actually the current efficiency of the oxide formation. The mass of porous alumina, m_p is related to the thickness h, via the density, $d_{Al_2O_3}$ and the porosity, p

$$d_{Al_2O_3} = \frac{m_p}{V_{ox}} = \frac{m_p}{S_{ox}(1-p)h} \tag{4}$$

where S_{ox} is the oxide surface area. The thickness of the porous oxide vs. current density combining Eqs. (2), (4) is

$$h = \frac{M_{Al_2O_3}\; i\; T_{o^{2-}}\; t}{z\,F\; d_{Al_2O_3}(1-p)\; S} = \frac{M_{Al_2O_3}\; j\; T_{o^{2-}}\; t}{z\,F\; d_{Al_2O_3}(1-p)} \tag{5}$$

and finally, the rate of growth R_p is obtained as a function of the current density:

$$R_p = \frac{dh}{dt} = \frac{M_{Al_2O_3}\; j\; T_{o^{2-}}}{z\,F\; d_{Al_2O_3}(1-p)} \tag{6}$$

In Fig. 4, the obtained growth rate R_p versus current density j is plotted for anodizations under 40 and 50 V at various temperatures. For the calculation of the current density j, the steady state value of the current was taken into account (see Fig. 3). According to the preceding analysis, the slope λ of the linear fit to the experimental points corresponds to

$$\lambda = \frac{M_{Al_2O_3}\; T_{O^{2-}}}{z\,F\; d_{Al_2O_3}\;(1-p)} \tag{7}$$

Using Eq. (7), the current efficiency for oxide formation T_O^{2-} is estimated, provided that the porosity and density of alumina are the same for all samples. The porosity of the PAMs has been reported to be depended on the time and the temperature of anodization under prolonged time and relatively high temperature due to dissolution mechanisms of the pore wall [28]. However, under the mild anodization conditions of the present work, the porosity was estimated from SEM images to 20 ± 2 % for all samples prepared under 40 V and 16 ± 2 % for samples anodized under 50 V at different temperatures.

On the other hand, it was recently suggested that porous formation is due to stress gradients at the barrier layer and not due to alumina dissolution [29, 30]. This was experimentally confirmed by the observation of tungsten tracers

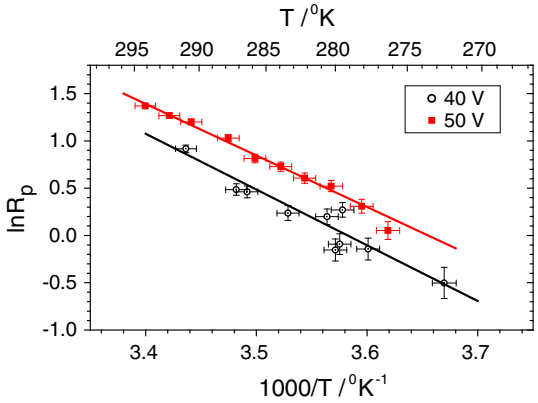

Fig. 5 Arrhenius-type plot of thickness growth rate R_p versus 1000/T of aluminum samples anodized at 40 and 50 V in 0.3 M oxalic acid in the temperature range of −0.5 upto 20 °C

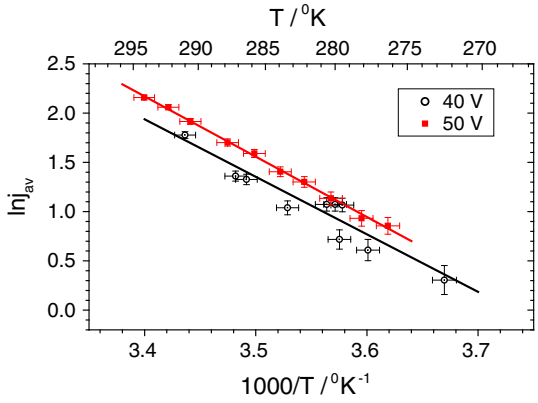

Fig. 6 Arrhenius-type plot of anodization average current density j_{av} versus 1000/T of aluminum samples anodized at 40 V in 0.3 M oxalic acid in the temperature range of −0.5 upto 18 °C and for samples anodized at 50 V in 0.3 M oxalic acid in the temperature range of 2–20 °C

dragged by the oxide which flowed toward the pore wall [31]. It is therefore apparent that the porosity depends mostly on the oxide displacement, rather than the chemical dissolution of the oxide, a procedure with very low formation enthalpy $\Delta H = -1675.7$ kJ mol^{-1} [22]. Small deviations in porosity due to chemical dissolution are possible either after long anodization times or at high temperatures [32].

From the slope of the graph R_p versus j (Fig. 4) and the above mentioned values for the alumina density $d_{Al_2O_3}$ and porosity p, the current efficiency was estimated to 53 and 65 % for samples prepared under 40 and 50 V, respectively, in a good agreement with previously published results [33]. Notably, the linear behavior depicted in Fig. 4 implies a constant transport number T_O^{2-}, for each value of anodization voltage (potentiostatic conditions) which is independent of temperature. From a practical point of view, the linear dependence of R_p versus j provides a very useful tool for in situ controlling the thickness of PAMs during the fabrication process.

In the framework of the present study, the effect of the solution temperature on the alumina growth rate was also investigated.

The linear behavior of lnR_p versus 1000/T shown in Fig. 5 implies an Arrhenius-type relation between the thickness growth rate and the temperature. Assuming that the reaction rate for the alumina formation is a pseudo-first order reaction (the concentration of Al^{3+} is in abundance), the growth rate is given by Eq. (8):

$$R_p = \frac{dh}{dt} \sim r \tag{8}$$

where r is the chemical reaction rate for the pure alumina formation given by Eq. (9):

$$r = A_o e^{-\frac{E_a}{RT}} \tag{9}$$

where R is the universal gas constant, E_a is the activation energy, and A_0 is a constant. Thus, the activation energy can be calculated from the slope of the linear fit of the plot lnR_p versus 1000/T as shown in Fig. 5.

In Fig. 6, the average current density, j_{av}, instead of the steady state current density, j, is used in the Arrhenius-type plot lnj_{av} versus 1000/T (although the two values do not differ significantly). This is justified from the fact that the thickness growth rate R_p is also a time averaged value derived from the final thickness over the total duration of the anodization. The mean activation energy resulting from Figs. 5, 6 for 40 V is 49 kJ mol^{-1} (0.51 eV), while this mean value in the case of 50 V is 48 kJ mol^{-1} (0.50 eV) which are in good agreement with the value of 0.52 eV reported in the literature [34].

Different experimentally determined activation energies E_a are reported in the literature between anodizations carried out in oxalic, phosphoric, and sulfuric acid. For anodization under potentiostatic conditions (100–150 V) in H_3PO_4, the activation energy was found equal to 75.2 kJ mol^{-1} [35]. (The higher the value of the activation energy, the slower a reaction proceeds). It is evident that the reaction of the electrolyte anions with the aluminum will determine the porous alumina formation rate, and this explains the different values of the growth rate when various acids are used as electrolytes for anodization (oxalic, phosphoric, sulfuric etc.). The increase in the value of $T_{O^{2-}}$ (higher growth rate) with the applied voltage (Fig. 4) implies a direct relationship of the available oxygen anions per unit time with the number of incorporated anions [36]. The incorporation rate increases with the applied voltage [37, 38]. The calculation method for oxygen transport number proposed in the present work which is based on measuring the current in the external circuit is direct and

more accurate, avoiding errors induced in methods using tracers [39].

5 Conclusions

In the present work, the effect of current density on the growth rate of porous alumina has been investigated in detail. Using the described electrochemical cell, a number of samples have been prepared under potentiostatic conditions (40 and 50 V in 0.3 M oxalic acid) at different temperatures, and the growth rate has been assessed by SEM analysis. It is found that the growth rate increases linearly with the current density; therefore, this is a useful parameter in order to control the final thickness of the membrane in a universal way. This linear dependence implies a constant value of current efficiency for oxide formation, which for the above conditions was found equal to 53 and 65 % for 40 and 50 V, respectively, and independent of temperature. Moreover, the rate of alumina growth exhibits an Arrhenius-type behavior with the temperature, which allows the estimation of a mean value for the activation energy E_a of alumina formation. Notably, a very close value for E_a can be deduced from the $\ln j_{av}$ versus $1000/T$ plot without the need of using SEM analysis for thickness determination. The estimated mean value of E_a equals to 48.5 kJ mol^{-1} and the dependence of this value, as reported in the literature, upon the acid used, favors models that focus on the role of the electrolyte anions such as the "viscous" flow model. Further investigation is needed in order to clarify the role of these anions on the growth of the porous oxide.

Acknowledgments This work was financially supported by *"Karatheodori 2010"* action, funded by the research committee of the University of Patras. Samples were characterized using the SEM of the SEM-Lithography group of the Polytechnic School of the University of Patras.

References

1. Yayoi K, Jinno M, Fujikawa R, Baryshev A, Khanikaev A, Shin KH, Uchida H, Inoue M (2007) Fabrication of high-quality two-dimensional photonic crystals based on porous alumina. Trans Elec Electron Eng 2(4):463–467
2. Hernadez- Velez M, Pirota KR, Paszti F, Navas D, Climent A, Vazquez M (2005) Magnetic nanowire arrays in anodic alumina membranes: rutherford backscattering characterization. Appl Phys A 80:1701–1706
3. Wang Z, Brust M (2006) Fabrication of nanostructure via self-assembly of nanowires within the AAO template. Nanoscale Res Lett 2(1):34–39
4. Koutsioubas GA, Spiliopoulos N, Anastassopoulos D, Vradis A, Priftis GD (2008) Nanoporous alumina enhanced surface plasmon resonance sensors. J Appl Phys 103:094521
5. Karagiovanaki S, Koutsioubas A, Spiliopoulos N, Anastassopoulos DL, Vradis AA, Toprakcioglu C, Siokou AE (2010) Adsorption of block copolymers in nanoporous alumina. J Polym Sci, Part B 48(14):1676–1682
6. Koutsioubas AG, Spiliopoulos N, Anastassopoulos DL, Vradis AA, Priftis GD (2009) On the implementation of nano-structured materials in surface plasmon resonance sensors. Mater Sci Eng, B 165(3):270–273
7. Koutsioubas AG, Spiliopoulos N, Anastassopoulos DL, Vradis AA, Toprakcioglu C (2009) Formation of polymer brushes inside cylindrical pores: a computer simulation study. J Chem Phys 131:044901
8. Dellis S, Christoulaki A, Spiliopoulos N, Anastassopoulos DL, Vradis AA (2013) Electrochemical synthesis of large diameter monocrystalline nickel nanowires in porous alumina membranes. J Appl Phys 114:164308
9. O'Suillivan JP, Wood CG (1970) The Morphology and Mechanism of Formation of Porous Anodic Films on Aluminium. Proc R Soc Lond A 317(1531):511–543
10. Sulka Grzegorz D, Stepniowski Wojciech J (2009) Structural features of self-organized nanopore arrays formed by anodization of aluminum in oxalic acid at relatively high temperatures. Electrochim Acta 54(14):3683–3691
11. Kashi MA, Ramazani A, Mayamai Y, Noormohammadi M (2010) Fabrication of self-ordered nanoporous alumina with 69–115 nm Interpore distances in sulfuric/oxalic acid mixtures by hard anodization. Jpn J Appl Phys 49:015202
12. Nielsch K, Choi J, Schwirn K, Wehrspohn RB, Gosele U (2002) Self-ordering regimes of porous alumina: the 10 porosity rule. Nano Lett 2(7):677–680
13. Keller F, Hunter SM, Robinson LD (1953) Structural features of oxide coatings on aluminum. J Electrochem Soc 100(9):411–419
14. Lee W, Ji R, Gosele U, Nielsch K (2006) Fast fabrication of long-range ordered porous alumina membranes by hard anodization. Nat Mater 5:741–747
15. Parkhutik VP, Albella JM, Makushok YuE, Montero I, Martinez-Duart JM, Shershulskii VI (1990) Study of aluminum anodization in sulphuric and chromic acid solutions—I. Kinetics of growth and composition of oxides. Electrochimica Acta 35:955
16. Shimizu K, Habazaki H, Skeldon P, Thompson GE, Wood GC (2000) Migration of sulfate ions in anodic alumina. Electrochim Acta 45:1805
17. Mingliang Wang, Yinong Liu, Hong Yang (2012) A unified thermodynamic theory for the formation of anodized metal oxide structures. Electrochim Acta 62:424–432
18. Li F, Zhang L, Metzger RM (1998) On the growth of highly ordered pores in anodized aluminum oxide. Chem Mater 10(9):2470–2480
19. Thompson GE (1997) Porous anodic alumina: fabrication, characterization and applications. Thin Solid Films 297(1–2):192–201
20. Zhu X-F, Song Y, Liu L, Wang C-Y, Zheng J, Jia H-B, Wang X-L (2009) Electronic currents and the formation of nanopores in porous anodic alumina. Nanotechnology 20:475303
21. Zhu XF, Li DD, Song Y, Xiao YH (2005) The study on oxygen bubbles of anodic alumina based on high purity aluminum. Mater Lett 59(24–25):3160–3163
22. Wu Z, Richter C, Menon L (2007) A study of anodization process during pore formation in nanoporous alumina templates. J Electrochem Soc 154(1):E8–E12
23. Houser Jerrod E, Hebert Kurt R (2009) The role of viscous flow of oxide in the growth of self-ordered porous anodic alumina films. Nat Mater 8:415–420
24. Garcia-Vergara SJ, Iglesias-Rubianes L, Blanco-Pinzon CE, Skeldon P (2006) Mechanical instability and pore generation in anodic alumina. Proc R Soc A 462(2072):2345–2358
25. Olivier Comets, Voorhees Peter W (2012) The stress engendered by oxygen bubble formation in the electrolyte of solid oxide electrolysis cells. ECS Trans 41(33):123–128

26. Zaraska L, Sulka GD, Jaskula M (2011) Anodic alumina membranes with defined pore diameters and thicknesses obtained by adjusting the anodizing duration and pore opening/widening time. J Solid State Electrochem 15:2427–2436
27. Sulka Grzegorz D (2008) Nanostructured materials in electrochemistry. In: Ali Eftekhari (ed) Highly ordered anodic porous alumina formation by self-organized anodizing. Wiley-VCH Verlag GmbH & Co, Weinheim, pp 1–116
28. Zaraska L, Stępniowski WJ, Ciepiela E, Sulka GD (2013) The effect of anodizing temperature on structural features and hexagonal arrangement of nanopores in alumina synthesized by two-step anodizing in oxalic acid. Thin Solid Films 534:155–161
29. Garcia-Vergara SJ, Skeldon P, Thompson GE, Habazaki H (2007) Stress generated porosity in anodic alumina formed in sulphuric acid electrolyte. Corros Sci 49(10):3772–3782
30. Jihun Oh, Thompson Carl V (2011) Abnormal anodic aluminum oxide formation in confined structures for lateral pore arrays. J Electrochem Soc 158:C71–C75
31. Garcia-Vergara SJ, Skeldon P, Thompson GE, Hashimoto T, Habazaki H (2007) Compositional evidence for flow in anodic films on aluminum under high electric fields. J Electrochem Soc 154:C540–C545
32. Bocchetta P, Sunseri C, Bottino A, Cappanneli G, Chiavarotti G, Piazza S, Di Quarto F (2002) Asymmetric alumina membranes electrochemically formed in oxalic acid solution. J Appl Electrochem 32(9):977–985
33. Jessensky O, Müller F, Gösele U (1997) Self-organized formation of hexagonal pore arrays in anodic alumina. Appl Phys Lett 72(10):1173
34. Long Ba and Wei Sang Li (2000) Influence of anodizing conditions on the ordered pore formation in anodic alumina. J Phys D Appl Phys 33:2527
35. Han XY, Shen WZ (2011) Improved two-step anodization technique for ordered porous anodic aluminum membranes. J Electroanal Chem 655(1):56–64
36. Michalska-Domańska M, Norek M, Stępniowski WJ, Budner B (2013) Fabrication of high quality anodic aluminum oxide (AAO) on low purity aluminum- a comparative study with the AAO produced on high purity aluminum. Electrochim Acta 105:424–432
37. Stępniowski WJ, Norek M, Michalska-Domańska M, Bombalska A, Nowak-Stępniowska A, Kwaśny M, Bojar Z (2012) Fabrication of anodic aluminum oxide with incorporated chromate ions. Appl Surf ScI 259:324
38. Stępniowski WJ, Norek M, Michalska-Domańska M, Nowak-Stępniowska A, Bombalska A, Włodarski M, Bojar Z (2013) Incorporation of copper chelate ions into anodic alumina walls. Mater Lett 106:242–245
39. Mirzoev RA, Davydov AD, Stepanova NI (2011) The effect of electrolyte anions incorporated into anodic oxide films on the experimental transport numbers of ions. Electrochim Acta 56:4414